Journal of Dental Research
2015, Vol. 94(11) 1568–1574

DOI: 10.1177/0022034515599765
jdr.sagepub.com

Composition of Mineral Produced by Dental Mesenchymal Stem Cells

A.A. Volponi[1], E. Gentleman[1], R. Fatscher[2], Y.W.Y. Pang[1], M.M. Gentleman[2], and P.T. Sharpe[1]

Abstract

Mesenchymal stem cells isolated from different dental tissues have been described to have osteogenic/odontogenic-like differentiation capacity, but little attention has been paid to the biochemical composition of the material that each produces. Here, we used Raman spectroscopy to analyze the mineralized materials produced in vitro by different dental cell populations, and we compared them with the biochemical composition of native dental tissues. We show that different dental stem cell populations produce materials that differ in their mineral and matrix composition and that these differ from those of native dental tissues. In vitro, BCMP (bone chip mass population), SCAP (stem cells from apical papilla), and SHED (stem cells from human-exfoliated deciduous teeth) cells produce a more highly mineralized matrix when compared with that produced by PDL (periodontal ligament), DPA (dental pulp adult), and GF (gingival fibroblast) cells. Principal component analyses of Raman spectra further demonstrated that the crystallinity and carbonate substitution environments in the material produced by each cell type varied, with DPA cells, for example, producing a more carbonate-substituted mineral and with SCAP, SHED, and GF cells creating a less crystalline material when compared with other dental stem cells and native tissues. These variations in mineral composition reveal intrinsic differences in the various cell populations, which may in turn affect their specific clinical applications.

Keywords: MSCs, dental stem cells, dentine, cementum, Raman spectroscopy, mineralization

Introduction

Cells with properties of skeletal stem cells found in bone marrow have been identified in many stromal tissues and are described as mesenchymal stem cells (MSCs) if they meet certain in vitro criteria. When grown under mineralizing conditions, MSCs are capable of secreting a mineralized matrix that is used as an indication of the cells' "osteogenic" differentiation. Teeth and surrounding tissues are accessible sources of cells with MSC-like properties when cultured in vitro (Gronthos et al. 2000; Gronthos et al. 2002; Miura et al. 2003; Jo et al. 2007; Huang et al. 2009; Koyama et al. 2009; Waddington et al. 2009; Balic et al. 2010; Wang et al. 2012; Volponi and Sharpe 2013).

Cells with MSC properties can be isolated from dental pulp tissue of exfoliated deciduous teeth, known as SHED cells (i.e., stem cells from human-exfoliated deciduous teeth; Miura et al. 2003; Wang et al. 2012), or different parts of permanent (adult) teeth. Extracted permanent teeth can yield cells from adult dental pulp (i.e., DPA [dental pulp adult] cells; Gronthos et al. 2000; Gronthos et al. 2002; d'Aquino et al. 2007), the apical papilla of the developing root SCAP (i.e., stem cells from apical papilla; Sonoyama et al. 2006), and periodontal ligament (PDL; McCulloch et al. 1985; Seo et al. 2004). Remnants of gingival tissue are present on extracted teeth as a potential source of gingival fibroblasts (GF; Fournier et al. 2010; Mitrano et al. 2010; Wada et al. 2011; Hsu et al. 2012). MSCs can also be obtained from dental implant sites, where aspirated drilled bone chips can be collected (i.e., BCMP [bone chip mass population] cells; Park et al. 2012).

Previous studies confirmed that MSCs derived from different dental/oral tissues are capable of forming mineralized material in vitro (Gronthos et al. 2002; Miura et al. 2003; Seo et al. 2004; Sonoyama et al. 2006; Huang et al. 2009; Mitrano et al. 2010; Park et al. 2012), but little attention has been paid to the extent to which their composition resembles that of mineralized dental tissues formed in vivo. This is, however, an important consideration when these cells are used in regenerative dentistry approaches, since small variations in tissue composition and even minor differences in mineral crystallinity

[1]Craniofacial Development and Stem Cell Biology, Dental Institute, Kings College London, London, UK
[2]Materials Science and Engineering Department, State University of New York, Stony Brook, NY, USA

Corresponding Authors:
M.M. Gentleman, Materials Science and Engineering Department, State University of New York, Stony Brook, Heavy Engineering Building, Rm. 120, Stony Brook, NY 11794, USA.
Email: molly.gentleman@stonybrook.edu
P.T. Sharpe, Craniofacial Development and Stem Cell Biology, Dental Institute, Kings College London, Floor 27, Guy's Hospital, London, SE1 9RT, UK.
Email: paul.sharpe@kcl.ac.uk

and the substitution environment can have profound effects on tissue function (Mandiar and Morris 2010; Morris and Mandiar 2011).

In this study, we used Raman spectroscopy to examine the composition of mineralized nodules formed in vitro from 6 types of cells isolated from human teeth and supporting tissues, and we compared their composition with that of dentine, enamel, and cementum. The results reveal differences in the material formed and may have consequences for their use in tissue engineering.

Material and Methods

Patient Recruitment

This study was approved by the Ethical Committee for Human Studies at Guy's Hospital, London, UK. Informed consent was obtained from donors who provided aspirated material following dental implant placement (to isolate BCMP cells) and extracted teeth for clinical reasons (to isolate DPA, GF, SCAP, and PDL cells). Parental consent was obtained in case of children (to isolate SHED cells), where deciduous teeth were extracted for clinical reasons. The patients were recruited at the oral surgery and restorative dentistry departments at Guy's Hospital.

All the samples were transferred into sterile vials of hypotonic phosphate-buffered saline solution and transported to the Craniofacial Development and Stem Cell Biology laboratory for processing.

Isolation and Establishment of Primary Cells

The roots of the deciduous teeth were partially resorbed, and the dental pulp chamber was easily accessible. Extracted remnants of deciduous dental pulp were enzymatically treated to obtain SHED cells (Fig. 1A).

DPA cells were isolated from dental pulp tissue of extracted permanent teeth. Following a cut just below the enamel-cementum junction, the dental pulp tissue was accessed from coronal and root portions of the pulp chamber. The tissue was minced and further enzymatically treated. For PDL cells, PDL was gently separated/scraped from the middle third of the root surface after tooth extraction. Root apical papilla was gently separated from the surface of growing roots where the apical papilla region was present; then, it was minced and digested in an enzymatic solution to obtain the SCAP population of cells.

Enzymatic treatment and cell culture. Tissue (dental pulp, apical papilla, or PDL region) was digested in a solution of collagenase I (3 mg/mL; Worthington Biochemical, Freehold, NJ, USA) and Dispase (4 mg/mL; Roche Molecular Biochemicals, Pleasanton, CA, USA) for 1 h at 37 °C to digest the tissue. Following centrifugation (600 × *g*, 2,000 rpm for 5 min), cell pellets were obtained and supernatants aspirated. Single-cell suspensions were obtained by passing cells through narrow Pasteur pipettes and 70-µm cell strainers (Falcon, BD Labware, Franklin Lakes, NJ, USA). Cells were plated at a density of 5×10^4 cells/cm^2 and cultured in MSC basal medium (MSCBM; Lonza, Basel, Switzerland).

To obtain GF, the remnants of gingival tissues attached to extracted teeth were minced, incubated overnight at 4 °C with Dispase (2 mg/mL) to separate the epithelial and spinous layers. The next day, the epithelial layer was removed and the spinous part minced into fragments and digested with collagenase IV (4 mg/mL; Worthington Biochemical) at 37 °C for 2 h. The dissociated cell suspension was filtered through a 70-µm cell strainer (Falcon, Heidelberg, Germany), and a single-cell suspension was obtained. Cells were grown in MSCBM medium.

The aspirated material following dental implant placement was collected in a filter trap (AstraTech, Waltham, MA, USA) on a suction line. This material was transferred into media containing α-MEM (Lonza) supplemented with 2% antibiotic-antimicotic on ice. Samples were transferred to 25 cm^2 of tissue culture flasks with 3 mL of MSCBM and 1 mg/mL (w/v) collagenase II. Enzymatic treatment was aided by placing the material in a 200-rpm shaking incubator for 1 to 2 h at 37 °C until the material started to become less compact. Cell pellets were obtained and resuspended in MSCBM, plated on a 25-cm^2 culture flask, and incubated at 37 °C in a 5% CO_2 incubator. All cells were used at P2 (Fig. 1A).

Mineralization-inducing Differentiation

Cells were seeded at a density of 2.0×10^5 cells/well onto 0.25-cm^2 MgF_2 substrates (MTI Corporation, Richmond CA, USA), with an optically clear weak Raman scattering material (Gentleman et al. 2009) placed in 12-well plates or onto the well surface (Fig. 1B). Control samples were grown in MSCBM. Triplicates of wells were examined for each experimental group. When cells reached 80% to 90% confluence, the medium in the experimental group was changed, and cells were grown in mineralization-inducing medium with the STEMPRO Osteogenesis Differentiation Kit (Invitrogen, Waltham, MA, USA), while the control group was grown in MSCBM.

Medium was changed every 2 d. After culturing for 28 d, cultures on well plates were fully washed with phosphate-buffered saline and fixed with phosphate-buffered formalin for 10 min. The fixed cells were washed with distilled water, after which they were stained with 1% alizarin red S (diluted in distilled water) for 20 min. The remaining dye was washed out with distilled water, and the cells were washed again. Finally, the cells were air-dried, and images of the stained cells were captured with an Olympus CK40 using ProGres CT5 CapturePro 2.8.8.2 Jenoptic Optical Systems Software (Jena, Germany).

Raman Spectroscopy

After culture for 28 d on MgF_2 substrates in mineralization-inducing medium, nodules formed by cells were air-dried and

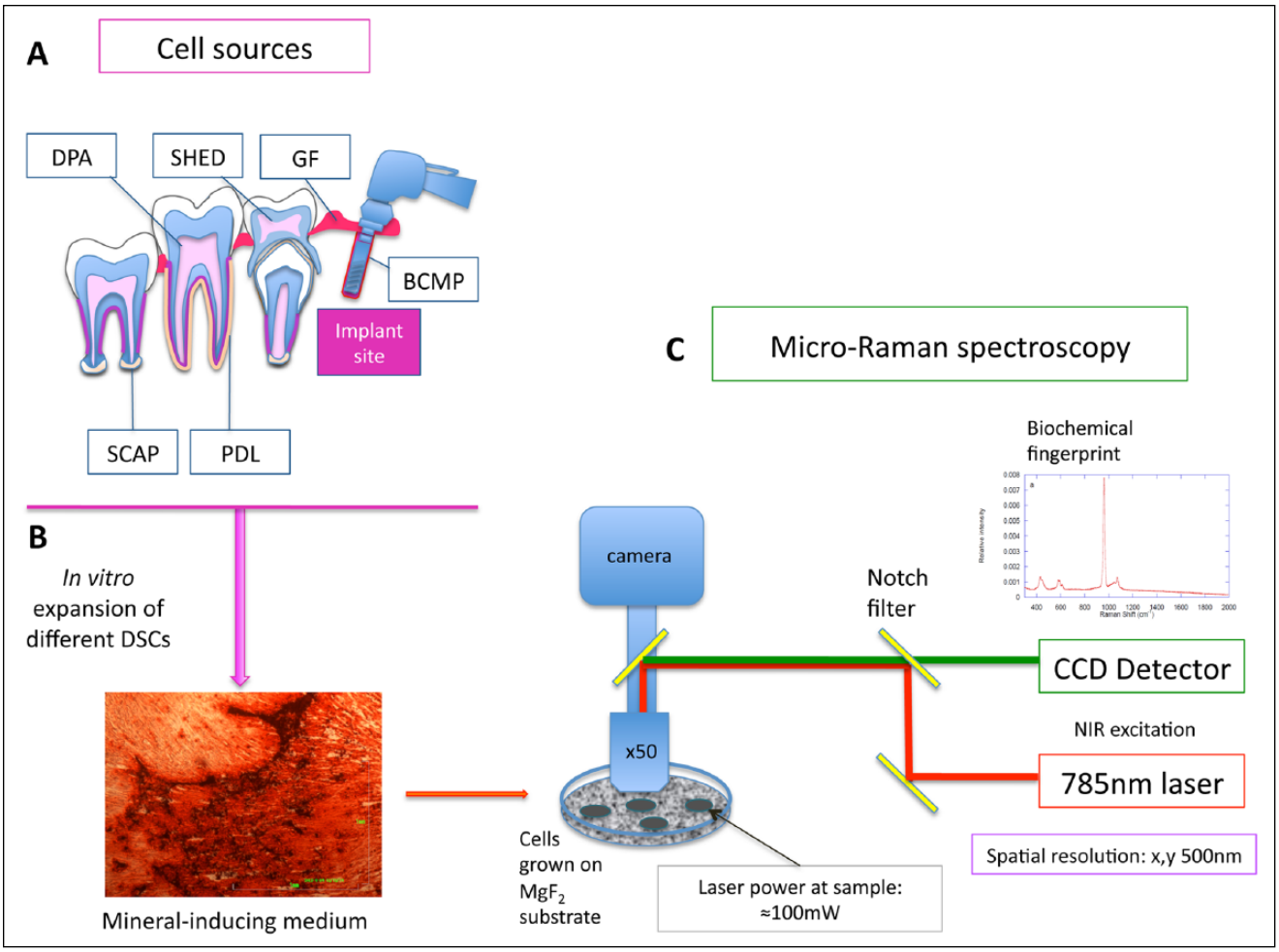

Figure 1. Schematic representation of pathway of analysis of cell populations. Different mesenchymal cells were isolated from different dental and supporting tissues (**A**). After their in vitro expansion, the cells were grown in mineral-inducing media for 28 d. All cells formed minerals in vitro that were confirmed with alizarin red staining, marking the calcium deposition (**B**). Cells were grown on MgF_2 coverslips (to facilitate Raman spectral analysis) and analyzed by micro-Raman spectrometer outfitted with a Leica microscope and 785-nm in-line diode laser (**C**). BCMP, bone chip mass population; CCD, charge-coupled device; DPA, dental pulp adult; GF, gingival fibroblast; NIR, near infrared; PDL, periodontal ligament; SCAP, stem cells from apical papilla; SHED, stem cells from human-exfoliated deciduous teeth.

stored in a dessicator prior to analysis. Raman spectra were collected on a Renishaw inVia micro-Raman spectrometer with a Leica microscope and 785-nm in-line diode laser (Fig. 1C). A 1,200-line/mm grating was used to maximize spectral resolution (~1 cm^{-1}). Wavelength and intensity calibrations were completed with the 520-cm^{-1} Si-band from a silicon standard internal to the spectrometer. For each experimental group, the collection time and laser intensity were adjusted to obtain an optimal signal-to-noise ratio. Following collection, spectra were processed with Wire 4.1 software. Spectral areas were normalized to an area of 1 and an offset baseline subtracted. Peaks were fit with full Voigt curves from which peak intensities, full width at half maximum (FWHM), and peak position were determined. Mineral-to-matrix ratio was calculated by dividing the area under the PO_4^{3-} v_1 peak at ~960 cm^{-1} by the area under the peak centered at ~1,660 cm^{-1} (attributed to amide I).

To identify subtle differences among spectra, an average Raman spectrum was produced for each experimental group and input into CAMO Unscrambler software (Oslo, Norway) and a principal component analysis completed. The following terms were identified as having significant variance:

Peak intensities: PO_4^{3-} (v_1, v_2, v_3, v_4), CO_3^{2-} (v_1), amide III, amide I, and C-H bending
Peak positions: PO_4^{3-} (v_1, v_2, v_3, v_4), CO_3^{2-} (v_1)
Peak FWHM: PO_4^{3-} (v_1, v_2, v_3, v_4), CO_3^{2-} (v_1), amide III, amide I, and C-H bending

Because the number of principal components identified as significant was large, the following criteria were applied to decrease the number of terms and reduce redundancy. Intensity changes were interpreted as being due to the amount of matrix secreted by cells/mineralized nodule thickness rather

than differences in the material composition—because more material will create more Raman scatter and, thus, more counts without a fundamental change in mineral composition. Positional shifts and variation in FWHM of the phosphate and carbonate peaks were attributed to changes in the local crystallinity and defect environments and were assumed to correlate with compositional variations. The strongest phosphate PO_4^{3-} (v_1) and carbonate CO_3^{2-} (v_1) modes were selected to act as representative modes for those lattice sites, and their behaviors were further studied.

Mineral-to-matrix ratios were analyzed by analysis of variance with post hoc Tukey test. Differences were considered significant at $P < 0.05$.

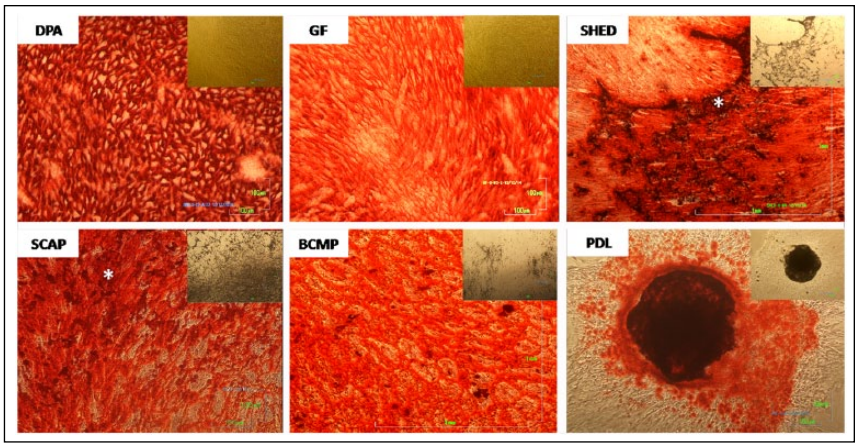

Figure 2. Alizarin red staining of different dental stem cells marking the deposition of calcium and showing different patterns of deposition throughout the experimental wells. Phase-contrast images of the cells are embedded in the upper right corner of alizarin red–stained images accordingly. DPA cells displayed beehive-like, homogeneously spread deposition of mineral when compared with PDL cells, which displayed nodular deposition with dark-stained areas of high-density calcium deposition. GF showed deposition of mineral in a fiber-like pattern throughout the surface of the experimental wells, while BCMP showed more lamellar pattern of mineral deposition. SHED and SCAP showed deposition that was not homogeneous, displaying zones of "accumulation" (asterisks)—higher-density mineral randomly localized. BCMP, bone chip mass population; DPA, dental pulp adult; GF, gingival fibroblast; PDL, periodontal ligament; SCAP, stem cells from apical papilla; SHED, stem cells from human-exfoliated deciduous teeth.

Results

Osteogenic Differentiation

After 28 d in mineral-inducing (osteogenic) medium, dense deposits were observed in all 6 groups of cells (Fig. 2) but absent in controls (not shown). Alizarin red staining in all groups was positive, indicating the deposition of calcium, but variation in the pattern of deposition was evident (Fig. 2). DPA stem cells produced a beehive-like, homogeneously spread mineral layer, while PDL cells created nodules with high-density areas that stained dark red (black) and were surrounded by areas with no staining. SHED and SCAP cells deposited mineral inhomogeneously with zones of high-density accumulations. Alternatively, GF cells formed mineral in a fiber-like pattern, and BCMP cells produced a more lamellar pattern of mineral deposits.

Mineralized Matrix Analyses by Raman Spectroscopy

Raman spectra collected from dense nodules formed from all cells were marked by a strong peak associated with PO_4^{3-} ν_1 vibrations at ~960 cm^{-1}, confirming positive alizarin red staining for the presence of mineral. Nevertheless, dramatic differences were noted among the spectral signatures of the mineralized material created by each cell population, and all differed from that of native mineralized dental tissues (enamel, dentin, and cementum; Fig. 3A). For example, although all the cells produced a strong peak at ~960 cm^{-1}, its intensity relative to the amount of organic matrix produced varied, as DPA, PDL, and GF cells produced a material with a lower mineral-to-matrix ratio (intensity ratio of PO_4^{3-} ν_1 to amide I) as compared with BCMP, SCAP, and SHED cells (Fig. 3B). Additionally, peaks for matrix components, including Amide III (1,242 cm^{-1}) and C-H bending (1,446 cm^{-1}), varied widely with relatively large intensities in DPA and GF cells but smaller in BCMP. As previously reported, native human dentine and cementum produced Raman peaks indicative of both mineral and matrix components, while in enamel, matrix peaks were not detectable (Bartlett et al. 2006; Margolis et al. 2006; Fig. 3). Raman spectra for dentine and enamel from deciduous and permanent teeth showed similar features. All cells produced a material that was grossly more similar to dentine/cementum than enamel.

In addition to examining peak intensities as relative indicators of mineral and matrix content, we examined other factors of the mineral environment that may influence the quality and function of mineralized tissue. Plots comparing FWHM of the PO_4^{3-} ν_1 peak (indicator of mineral crystallinity), position of the PO_4^{3-} ν_1 peak (described as either a measure of crystallinity or stress in the crystal lattice), and carbonate-to-phosphate ratio (indicator of carbonate substitution into the apatite lattice) show how the mineralized material created by cells compare with one another and to that of native mineralized dental tissues.

Figure 4A shows the FWHM of the PO_4^{3-} ν_1 peak as a function of its position for all cell populations and native dental tissues. Spectra collected from enamel, dentine, and cementum tended to be less variable than those collected from the cell sources, as is evident from the tight clustering of measurements. Spectra for enamel also clustered away from other native dental tissues and mineral formed by cells because it was more crystalline, as indicated by the lower FWHM of the 960 cm^{-1} peak. Spectra of mineralized nodules produced by

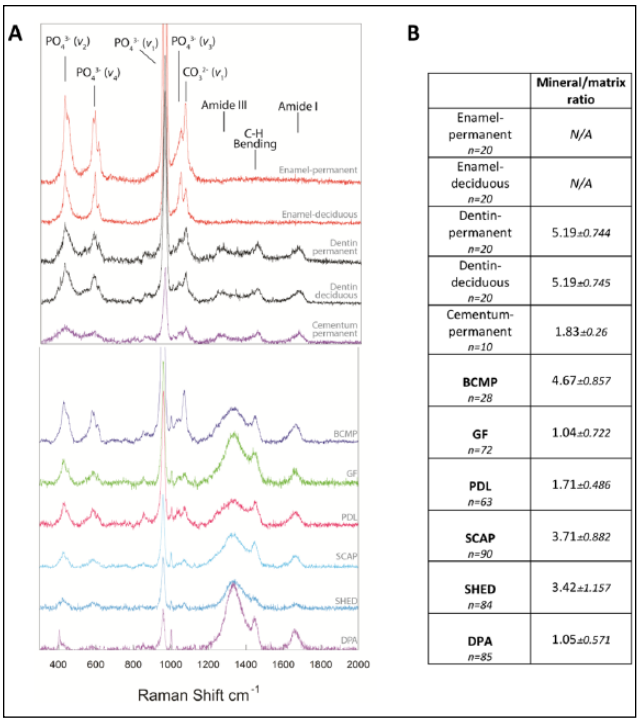

	Mineral/matrix ratio
Enamel-permanent n=20	N/A
Enamel-deciduous n=20	N/A
Dentin-permanent n=20	5.19±0.744
Dentin-deciduous n=20	5.19±0.745
Cementum-permanent n=10	1.83±0.26
BCMP n=28	4.67±0.857
GF n=72	1.04±0.722
PDL n=63	1.71±0.486
SCAP n=90	3.71±0.882
SHED n=84	3.42±1.157
DPA n=85	1.05±0.571

Figure 3. Representative Raman spectra and mineral to matrix ratios for native dental tissues and material formed by dental stem cells. (**A**) Average Raman spectra collected from native human dental tissue and mineralized nodules formed from dental stem cells. All spectra were intensity normalized to 1 and offset along the vertical axis. Peaks of interest associated with mineral and matrix components are indicated. (**B**) Mean mineral-to-matrix ratio values calculated for native dental tissues and material formed by dental stem cells. Mineral-to-matrix ratio was calculated by dividing the area under the ~960-cm^{-1} peak by the area under the amide I peak at ~1,660 cm^{-1}. As matrix peaks were not detected in native enamel, mineral-to-matrix ratios were not calculated. All comparisons of mineral-to-matrix ratios were significant at the $P < 0.05$ level, with the exception of the following: dentin-permanent vs. dentin-deciduous, dentin-permanent/dentin-deciduous vs. BCMP, cementum-permanent vs. GF/PDL/DPA, GF vs. DPA, and SCAP vs. SHED. BCMP, bone chip mass population; DPA, dental pulp adult; GF, gingival fibroblast; PDL, periodontal ligament; SCAP, stem cells from apical papilla; SHED, stem cells from human-exfoliated deciduous teeth.

PDL and BCMP cells clustered closely with that from dentin, suggesting that the phosphate environments were similar. Similarly, spectra from permanent cementum showed a similar phosphate structure to that obtained from DPA. SHED, GF, and SCAP cells produced a mineral that was more amorphous when compared with other dental cells and native dental tissues, as indicated by the larger FWHM of the 960 cm^{-1} peak. Moreover, the PO_4^{3-} ν_1 peak position of the mineral formed by SCAP and SHED tended to be at a lower wave number when compared with that of other groups, which may reflect a more amorphous mineral or less stress in the mineral lattice.

A plot detailing carbonate substitution into the apatite lattice as a function of the PO_4^{3-} ν_1 peak position is shown in Figure 4B. Carbonate substitution into the apatite lattice was variable in the mineralized nodules produced by cells and native dental tissues, as indicated by the relatively large vertical scatter of points (with the exception of BCMP cells). Nevertheless, dentin, enamel, SCAP, SHED, GF, and PDL all produced mineral with similar degrees of carbonate substitution. DPA, however, produced a mineral with a relatively large degree of carbonate substitution, which was similar to that detected in native permanent cementum. In native bone tissue samples, carbonate substitution has been associated with the age of the tissue and correlated with poorer mechanical properties (Akkus et al. 2004) but may also reflect distortions to the crystal lattice associated with other factors.

Discussion

Raman spectroscopy is increasingly recognized as an important tool to understand the biochemical changes in mineral composition and structure. As a technique, it can be used with fresh, fixed, or embedded specimens, offering a noninvasive measurement. Raman spectroscopy has been applied to the study of stem cells and the matrix secreted by differentiated cells (Chan et al. 2009; Gentlemen et al. 2009; Downes et al. 2011). The mineral phase that is found in native tooth tissues (enamel, dentin, and cementum) produces characteristic peaks attributable to phosphate vibrations, likely in the form of hydroxyapatite, and observed at ~960 cm^{-1} (Boskey 2007). In these mineral structures, CO_3^{2}-substituted apatite nanocrystals are oriented with their long axes parallel to the axes of collagen fibrils, the major organic matrix component. Other proteins are also present playing roles in cell-matrix interactions, cell signaling, and control of mineralization (Wiesmann et al. 2005; Margolis et al. 2006; Boskey 2007).

We analyzed native mineralized tissues of teeth (enamel, dentin, and cementum) and used these measurements as comparison points for the biochemical characteristics of mineralized tissue formed in vitro by different dental mesenchymal cells grown in osteogenic medium. Human cell populations were isolated from different parts of the tooth and surrounding tissues that have been shown to have MSC properties in vitro (Gronthos et al. 2002; Miura et al. 2003; Seo et al. 2004; Sonoyama et al. 2006; Huang et al. 2009; Mitrano et al. 2010; Park et al. 2012). In addition, we included a source of cells (BCMP) isolated from the bone chip material obtained during dental implant procedures.

We were unable to detect peaks for organic matrix in the enamel. This was expected as 1) enamel does not contain collagen and 2) proteins constitute only a small proportion of mature enamel's composition (Bartlett et al. 2006; Margolis et al. 2006).

Quantitative analysis of Raman spectra collected from the mineralized material produced by cells in vitro can be performed (Timlin et al. 1999) by calculating peak intensity ratios, such as the mineral-to-matrix ratio and carbonate-to-phosphate ratio. Our cells were air-dried before analysis, as our previous work has shown that drying has little effect on the composition of mineralized nodules (Evans et al. 2012).

When analyzed in relation to the native mineralized tissue, the mineral formed in vitro by BCMP had a similar mineral-to-matrix ratio to that of dentin, while DPA and GF were similar to that of permanent cementum. However, in addition to examining peak

intensities as relative indicators of mineral and matrix content produced by dental cells, we aimed to examine other factors of the mineral environment that may influence quality and function of mineralized tissue. Plots comparing the carbonate-to-phosphate ratio (Fig. 4), the position of the PO_4^{3-} ν_1 peak (described as either a measure of crystallinity or stress in the crystal lattice), and the FWHM of the PO_4^{3-} ν_1 peak (indicator of mineral crystallinity; Fig. 4A) show how the mineralized material created compares with that of native mineralized dental tissues. Although there was overlap in mineral composition among different cell populations, there were several clear distinctions. Based on the mineral parameters measured, DPA produced material that was most akin to cementum and differed from SHED cells, which produced mineral with a composition more similar to SCAP cells. Surprisingly, the mineral produced by GF cells was more similar in composition to dentine than that produced by any of the other cell populations.

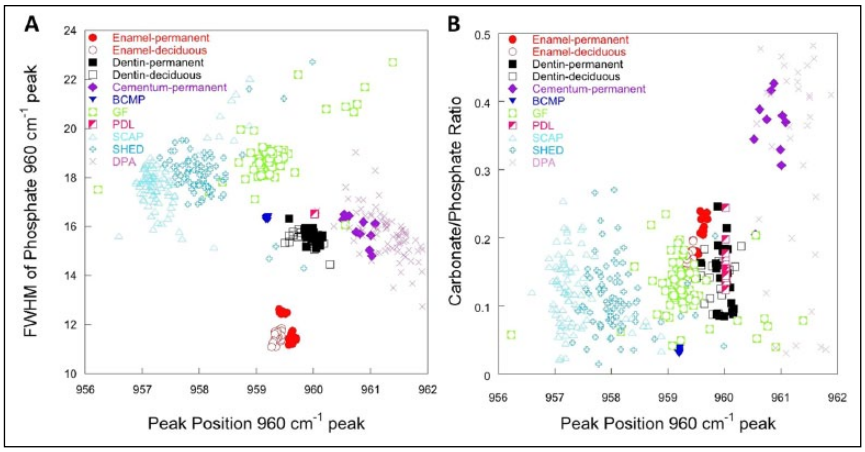

Figure 4. Component analysis plots for native dental tissues and material formed by dental stem cells. (**A**) Characteristic full-width half maximum of the phosphate PO_4^{3-} ν_1 stretching modes as a function of the peak position of the same for the mineral components of native enamel, dentin, and cementum, as well as BCMP, GF, PDL, SCAP, SHED, and DPA. Strong overlaps in these mineral variables correspond to correlations in the stress state and crystallinity in the native tissues and mineral deposits. Nodules from PDL and BCMP correlated strongly with native dentin, while those from DPA corresponded to that of native cementum. (**B**) Carbonate substitution calculated by measuring the area under the CO_3^{2-} ν_1 with respect to the area under the PO_4^{3-} ν_1 mode is plotted as a function of the position of the PO_4^{3-} ν_1 mode. Native dentin, native enamel, SCAP, SHED, GF, and PDL all produce similar levels of carbonate substitution, while DPA and native cementum produce somewhat higher levels. BCMP, bone chip mass population; DPA, dental pulp adult; GF, gingival fibroblast; PDL, periodontal ligament; SCAP, stem cells from apical papilla; SHED, stem cells from human-exfoliated deciduous teeth.

All cells were grown in mineralization-inducing environment, and mineral deposition could be clearly observed after 28 d in culture. Different patterns of mineral deposition were observed after alizarin red staining (Fig. 2), indicative of different biological "fingerprints."

While most histochemical stains indicate presence of calcium and phosphate ions, Raman spectral signatures provide a more in-depth characterization of the mineralized material produced by cells. Here, we determined that all cells produced a carbonate-substituted apatite-like mineral template on an organic matrix, but its characteristics varied depending on cell source, and none perfectly matched that of native dental tissues. By investigating the biochemical signatures of mineral deposited by all 6 cell sources isolated from dental tissues, we conclude that the material that each creates differs from the others (Figs. 3, 4). These observations may have important implications for using these cells in regenerative medicine applications. For example, bone mineral composition, particularly changes in mineral crystallinity, can have profound effects on bone tissue mechanical properties and, thus, function (Akkus et al. 2004). However, it is also possible that the differences in mineral composition detected in our in vitro system here could have no effect on clinical outcomes. Implanted tissues may be remodeled by native cells, or factors in the in vivo environment may differently direct stem cell differentiation and mineral formation. Further analyses of mineral created by cells implanted in vivo may shed light on this issue.

Our results show differences in the mineralization capacity of dental cells. Understanding the underlying potential of different cells derived from such accessible sources in forming biochemically different mineralized structures in vitro can enable their targeted usage in regenerative tissue engineering approaches.

Author Contributions

A.A. Volponi, R. Fatscher, contributed to data acquisition, drafted and critically revised the manuscript; E. Gentleman, contributed to data interpretation, drafted and critically revised the manuscript; Y.W.Y. Pang, contributed to data analysis, drafted and critically revised the manuscript; M.M. Gentleman, contributed to data interpretation and analysis, drafted and critically revised the manuscript; P.T. Sharpe, contributed to conception, design, and data analysis, drafted and critically revised the manuscript. All authors gave final approval and agree to be accountable for all aspects of the work.

Acknowledgments

We thank Prof. Richard Palmer and Dr. Chris Sproat from Guy's Hospital, King's College, London, UK, for their help in patient recruitment. We thank Riddhi Sharma, Mihnea Nicolescu, and Hasan Jamal for alizarin red staining images, as part of their MSC training in regenerative dentistry. E.G. is supported by a Research Career Development Fellowship from the Wellcome Trust. The authors declare no potential conflicts of interest with respect to the authorship and/or publication of this article.

References

Akkus O, Adar F, Schaffler MB. 2004. Age-related changes in physicochemical properties of mineral crystals are related to impaired mechanical function of cortical bone. Bone. 34(3):443–453.

Balic A, Aguila HL, Caimano MJ, Francone VP, Mina M. 2010. Characterization of stem and progenitor cells in the dental pulp of erupted and unerupted murine molars. Bone. 46(6):1639–1651.

Bartlett JD, Ganss B, Goldberg M, Moradian-Oldak J, Paine ML, Snead ML, Wen X, White SN, Zhou YL. 2006. Protein-protein interactions of the developing enamel matrix. Curr Top Dev Biol. 74:57–115.

Boskey A. 2007. Mineralization of bones and teeth. Elements. 3(6):385–391.

Chan J, Taylor D, Thompson D. 2009. The effect of cell fixation on the discrimination of normal and leukemia cells with laser tweezers Raman spectroscopy. Biopolymers. 91(2):132–139.

d'Aquino R, Graziano A, Sampaolesi M, Laino G, Pirozzi G, De Rosa A, Papaccio G. 2007. Human postnatal dental pulp cells co-differentiate into osteoblasts and endotheliocytes: a pivotal synergy leading to adult bone tissue formation. Cell Death Differ. 14(6):1162–1171.

Downes A, Mouras R, Bagnaninchi P, Elfick A. 2011. Raman spectroscopy and CARS microscopy of stem cells and their derivatives. J Raman Spectrosc. 42(10):1864–1870.

Evans ND, Swain RJ, Gentleman E, Gentleman MM, Stevens MM. 2012. Gene-expression analysis reveals that embryonic stem cells cultured under osteogenic conditions produce mineral non-specifically compared to marrow stromal cells or osteoblasts. Eur Cell Mater. 24:211–223.

Fournier BP, Ferre FC, Couty L, Lataillade JJ, Gourven M, Naveau A, Coulomb B, Lafont A, Gogly B. 2010. Multipotent progenitor cells in gingival connective tissue. Tissue Eng Part A. 16(9):2891–2899.

Gentleman E, Swain RJ, Evans ND, Boonrungsiman S, Jell G, Ball MD, Shean TA, Oyen ML, Porter A, Stevens MM. 2009. Comparative materials differences revealed in engineered bone as a function of cell-specific differentiation. Nat Mater. 8(9):763-770.

Gronthos S, Brahim J, Li W, Fisher LW, Cherman N, Boyde A, DenBesten P, Robey PG, Shi S. 2002. Stem cell properties of human dental pulp stem cells. J Dent Res. 81(8):531–535.

Gronthos S, Mankani M, Brahim J, Robey PG, Shi S. 2000. Postnatal human dental pulp stem cells (DPSCs) in vitro and in vivo. Proc Natl Acad Sci U S A. 97(25):13625–13630.

Hsu SH, Huang GS, Feng F. 2012. Isolation of the multipotent MSC subpopulation from human gingival fibroblasts by culturing on chitosan membranes. Biomaterials. 33(9):2642–2655.

Huang GT, Gronthos S, Shi S. 2009. Mesenchymal stem cells derived from dental tissues vs. those from other sources: their biology and role in regenerative medicine. J Dent Res. 88(9):792–806.

Jo YY, Lee HJ, Kook SY, Choung HW, Park JY, Chung JH, Choung YH, Kim ES, Yang HC, Choung PH. 2007. Isolation and characterization of postnatal stem cells from human dental tissues. Tissue Eng. 13(4):767–773.

Koyama N, Okubo Y, Nakao K, Bessho K. 2009. Evaluation of pluripotency in human dental pulp cells. J Oral Maxillofac Surg. 67(3):501–506.

Mandair G, Morris MD. 2010. Contributions of Raman spectroscopy to the understanding of bone strength. Bonekey Rep. 4:620.

Margolis HC, Beniash E, Fowler CE. 2006. Role of macromolecular assembly of enamel matrix proteins in enamel formation. J Dent Res. 85(9):775–793.

McCulloch CA. 1985. Progenitor cell populations in the periodontal ligament of mice. Anat Rec. 211(3):258–262.

Mitrano TI, Grob MS, Carrión F, Nova-Lamperti E, Luz PA, Fierro FS, Quintero A, Chaparro A, Sanz A. 2010. Culture and characterization of mesenchymal stem cells from human gingival tissue. J Periodontol. 81(6):917–925.

Miura M, Gronthos S, Zhao M, Lu B, Fisher LW, Robey PG, Shi S. 2003. SHED: stem cells from human exfoliated deciduous teeth. Proc Natl Acad Sci. 100(10):5807–5812.

Morris MD, Mandair GS. 2011. Raman assessment of bone quality clin orthop relat res. 469(8):2160–2169.

Park J, Kim JC, Kim Y, Choi S, Cho K, Im G, Kim B, Kim C. 2012. Acquisition of human alveolar bone-derived stromal cells using minimally irrigated implant osteotomy: in vitro and in vivo evaluations. J Clin Periodontol. 39(5):495–505.

Seo BM, Miura M, Gronthos S, Bartold PM, Batouli S, Brahim J, Young M, Robey PG, Wang CY, Shi S. 2004. Investigation of multipotent postnatal stem cells from human periodontal ligament. Lancet. 364(9429):149–55.

Sonoyama W, Liu Y, Fang D, Yamaza T, Seo BM, Zhang C, Liu H, Gronthos S, Wang CY, Wang S, et al. 2006. Mesenchymal stem cell-mediated functional tooth regeneration in swine. PLoS One. 1:e79.

Timlin J, Carden A, Morris M. 1999. Chemical microstructure of cortical bone probed by raman transects. Appl Spectrosc. 53(11):1429–1435.

Volponi AA, Sharpe PT. 2013. The tooth: a treasure chest of stem cells. Br Dent J. 215(7):353–358.

Wada N, Wang B, Lin NH, Laslett AL, Gronthos S, Bartold PM. 2011. Induced pluripotent stem cell lines derived from human gingival fibroblasts and periodontal ligament fibroblasts. J Periodontal Res. 46(4):438–447.

Waddington RJ, Youde SJ, Lee CP, Sloan AJ. 2009. Isolation of distinct progenitor stem cell populations from dental pulp. Cells Tissues Organs. 189(1–4):268–274.

Wang X, Sha XJ, Li GH, Yang FS, Ji K, Wen LY, Liu SY, Chen L, Ding Y, Xuan K. 2012. Comparative characterization of stem cells from human exfoliated deciduous teeth and dental pulp stem cells. Arch Oral Biol. 57(9):1231–1240.

Wiesmann HP, Meyer U, Plate U, Höhling HJ. 2005. Aspects of collagen mineralization in hard tissue formation. Int Rev Cytol. 242:121–156.